Indicators of propagation direction and relative depth in clastic injectites: Implications for laminar versus turbulent flow processes

S.L. Cobain[†], J. Peakall, and D.M. Hodgson
School of Earth and Environment, University of Leeds, Leeds LS2 9JT, UK

ABSTRACT

Clastic injectites are widely recognized in deep-water stratigraphic successions, although their sediment transport processes, propagation direction, and depth of injection are poorly constrained. Understanding how they form is important, as injectites are increasingly being recognized as significant components of sedimentary basin fills, yet are not predicted by standard sedimentary facies models. Here, analysis of features on the margins of exhumed clastic sills and dikes, and clasts within them, enables their genesis to be determined. A diverse array of diagnostic structures is found on the margins of injectites in the Karoo Basin, South Africa, where the net direction of injection and position of the parent sand are well constrained. Injectite margin features include mudstone clast–rich surfaces, planar or smooth surfaces, blistered surfaces, and parallel and plumose ridged surfaces. Combined, these features are critical in distinguishing injected sands, where injectites are strata concordant, from those of primary deposition. All features are indicative of propagation through brittle, very fine-grained sediments at depths where the applied shear stress is at least four times the tensile strength of the host rock. Additionally, the presence of parallel ridges, plumose ridges, and steps allows local fracture propagation to be constrained, and in turn injection direction. The features described provide evidence that sands were injected at considerable depth in closed fractures with limited capacity for flow dilution and turbulence enhancement. Calculated Reynolds numbers, lack of erosion at injectite walls, and the presence of mud clasts at the top and base of sills indicate that many flows were likely fully laminar during injection. The sedimentary features of these confined, relatively deep, laminar flow–induced injectites are very different from injectites that reach the surface and produce extrudites. Surface-linked injectites are associated with open conduits where a greater fraction of carrier fluid to particles can be accommodated, enabling highly turbulent, lower-concentration flows.

INTRODUCTION

Clastic injectites have been documented in many sedimentary environments (see Hurst et al., 2011; Ross et al., 2011, and references therein). Interest in injectites has increased as their significance for petroleum systems has been realized: they can serve as hydrocarbon reservoirs (e.g., Schwab et al., 2014) as well as dramatically change reservoir architecture and form fluid-migration pathways in a broad range of reservoirs (e.g., Dixon et al., 1995; Jolly and Lonergan, 2002). In the subsurface, reflection seismic data can help to constrain the large-scale architecture and in some cases the propagation direction of injection complexes (Hurst et al., 2003; Huuse et al., 2004; Cartwright et al., 2008; Vigorito et al., 2008; Szarawarska et al., 2010; Jackson et al., 2011), but flow direction and relative depth of formation are hard to interpret, even with the addition of core and outcrop analogues. Despite their importance, many of the underlying formation processes remain poorly understood, such as the mode of propagation and nature of sediment transport processes within these conduits. In particular, there has been considerable discussion on the nature of fluid flow during injection, especially whether flows are laminar or turbulent (Peterson, 1968; Taylor, 1982; Obermeier, 1998; Duranti, 2007; Hubbard et al., 2007; Hurst et al., 2011; Ross et al., 2014).

Here, we report detailed observations on the morphology and distribution of a wide array of structures on the margins of exhumed clastic injections. These observations are then integrated with the existing literature, including that pertaining to igneous dike and sill emplacement, to develop a model that considers the mechanisms and internal flow processes in operation during sand injection. We thus address the following fundamental questions: (1) Can injection propagation direction be determined using margin structures?; (2) Can injection depth be estimated?; and (3) What flow processes occur during injection? These questions support a discussion on sand injectite emplacement mechanisms, including the current debate on laminar versus turbulent flow and how this controls differences in injectite geometries and surface features.

SOURCES OF OVERPRESSURE, TRIGGER MECHANISMS, AND FRACTURE PROPAGATION: CURRENT UNDERSTANDING

The most commonly invoked triggering mechanisms for clastic intrusions are seismicity (Obermeier, 1998; Boehm and Moore, 2002; Obermeier et al., 2005) and overpressuring by rapid fluid migration into parent sands (Davies et al., 2006), rapid burial (Truswell, 1972; Allen, 2001), or instability of overlying sediments (Jonk, 2010). Seismicity as well as overpressure by rapid burial or unstable overlying sediments are associated with relatively shallow and commonly localized intrusion (Hurst et al., 2011; Bureau et al., 2014). Deeper, and in many cases larger-scale, injectites are thought to be related to compaction and/or the migration of fluids from a deeper source into a sealed sandstone body, causing an increase in pore pressure (Vigorito and Hurst, 2010; Bureau et al., 2014). Therefore at depth, in a seismically quiescent basin, pore fluid overpressure from compaction and/or migrating fluids can act as both the primer and the trigger for clastic injection.

Once triggered, clastic sills and dikes fill natural hydraulic fractures (Lorenz et al., 1991; Cosgrove, 2001; Jolly and Lonergan, 2002; Jonk, 2010) opening in a mode I propagation (Fig. 1) normal to the plane of least compressive stress (Delaney et al., 1986). Once opened, fracture propagation is maintained by a constant differential of pore fluid pressure between the

[†]E-mail: ee09sc@leeds.ac.uk
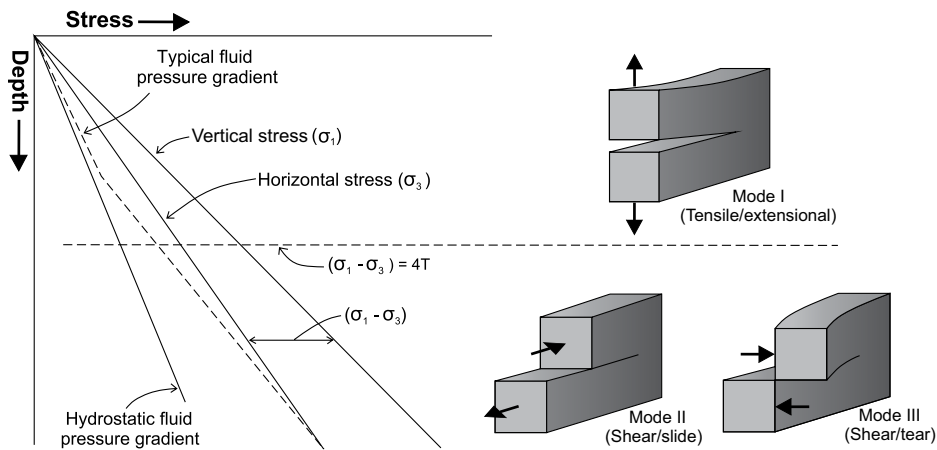
Figure 1. Plot of vertical and horizontal stress regimes in a tectonically relaxed basin. Differential stress increases with depth; at a depth where applied shear stress exceeds four times the tensile strength of the host rock, the type of fracture changes from extensional to shear. Mode I, II, and III type fractures are correlated with relative depth of formation. Adapted from Cosgrove (2001).

source bed and the tip of the propagating fracture. When the difference in pressure begins to balance, the fracture ceases to propagate and injection stops (Lorenz et al., 1991; Jonk, 2010). Initial failure can result from the development of a single critical fracture involving only a few primary flaws such as impurities, grain boundaries, inclusions, or microcracks (Aubertin and Simon, 1997) (Fig. 2, heterogeneous mudstone). The opening of a macroscopic crack, originating at one or more of these flaws, occurs when the stress intensity breaches the limit of the strength of the rock (Charlez, 1991). On a larger scale, even if stresses across bodies or whole beds of rock are uniform, small-scale stresses due to flaws or impurities at the tip of a propagating fracture may be uneven, causing irregularities in fracture direction and geometries (Lorenz et al., 1991; Aubertin and Simon, 1997) (Fig. 2, heterogeneous mudstone). Ben-Zion and Morrissey (1995) have shown that a fracture propagating through a heterogeneous medium (Fig. 2) continually interacts with random asperities and diverges as heterogeneities in the fracture energy are incorporated. Here, observations of features on the margins of exhumed injectites hosted in deep-marine deposits in the Karoo Basin are used in conjunction with fracture mechanics to interpret propagation direction and flow processes.

GEOLOGICAL BACKGROUND

The deep-water stratigraphy of the Laingsburg depocenter, southwestern Karoo Basin, South Africa, comprises a 1.8-km-thick shallowing-upwards succession passing from dis-

tal basin-floor (Vischkuil Formation; van der Merwe et al., 2010), through proximal basin-floor (Laingsburg Formation; Sixsmith et al., 2004) and channelized submarine-slope (Fort Brown Formation; Di Celma et al., 2011), to shelf-edge and shelf-delta deposits (Waterford Formation; Jones et al., 2013) (Figs. 3A and 3B). The Laingsburg and Fort Brown Formations comprise seven sand-prone units (units A to G) separated by regional mudstones, which signify shutdown of clastic input (Flint et al., 2011). Unit A (Laingsburg Formation) is further divided into six subunits (A1–A6), each bound by mudstones, which in turn relate to a regional shutdown of clastic input (Sixsmith et al., 2004; Prélat and Hodgson, 2013). The present study uses observations from an injectite-prone, 12-m-thick mudstone unit between units A5 and A6 at Buffels River, Laingsburg (Fig. 3B), where the source sand for clastic intrusions is the underlying unit A5, identified where dikes connect directly with sandstone beds. Figures 3C and D show the typical outcrop expression of the clastic sills and dikes.

RECOGNITION OF INJECTITES IN THE FIELD

Clastic injections in the Karoo Basin are fine-grained, well-sorted sandstones, much like the parent sandstones. Dikes are discordant with host strata, commonly at angles between 10° and 35°, though vertical dikes are also present, and range from <1 cm to several tens of centimeters in thickness and can be traced up to 20 m from the parent sand. Sills are concordant with host strata, although locally they step through stratigraphy

to form stepped sills, and range from a few centimeters to 1.3 m in thickness, and are hundreds of meters in length. Recognition criteria for clastic sills include the presence of distinctive features on top and base margins (Figs. 4 and 5) and the absence of depositional sedimentary structures such as planar or ripple cross-laminations or grain-size grading, although a faint banding is locally present toward top and base margins. In addition, injectites exposed in the Karoo Basin weather to a distinctive color and style, aiding field identification.

METHODOLOGY AND DATASET

Injectites were mapped at centimeter scale (Fig. 4B) along a 500-m-long, 12-m-thick southwest-northeast–trending exposure of a regional mudstone interval that separates sandstone-prone units A5 and A6 of the Laingsburg Formation at Buffels River, Laingsburg, which are interpreted as submarine lobe complexes (Prélat and Hodgson, 2013). Detailed sedimentologic and stratigraphic observations include logged sections, photographs, and dip and strike data (Fig. 4C). Eighteen logs were collected using the top of unit A5 and base of unit A6 as datums, as the mudstone in between has a constant thickness of 12 m across the entire panel.

EXTERNAL STRUCTURES AND MORPHOLOGY

Several different structures have previously been identified on the margins of exhumed clastic sills and dikes. Features include flute-like marks, grooves, rills, lobate scours, frondescent marks, and gutter marks (Peterson, 1968; Keighley and Pickerill, 1994; Parize and Friès, 2003; Surlyk et al., 2007; Kane, 2010; Hurst et al., 2011). Relief of such features ranges from millimeters to several meters in scale eroding into host stratigraphy. Small clasts of shale have been documented along dike margins in outcrop (e.g., Diller, 1890), with laminations within clasts parallel to those of the host stratigraphy (Newsom, 1903; Parize et al., 2007). Structures on the margins of clastic intrusions can form either during the fracturing and injection of the host rock by the intrusive body (Lutton, 1970; Cosgrove, 1995; Müller and Dahm, 2000) or through later erosion of the fractures by the injecting fluid-sediment mixture (e.g., Martill and Hudson, 1989; Hillier and Cosgrove, 2002; Hubbard et al., 2007; Hurst et al., 2011). If margin structures occur due to fracturing, in the absence of any later reworking by the intruded flows, then the morphology and distribution of structures on injectite margins can be used to infer the properties of the host rock and sediment, and their interaction, at the time
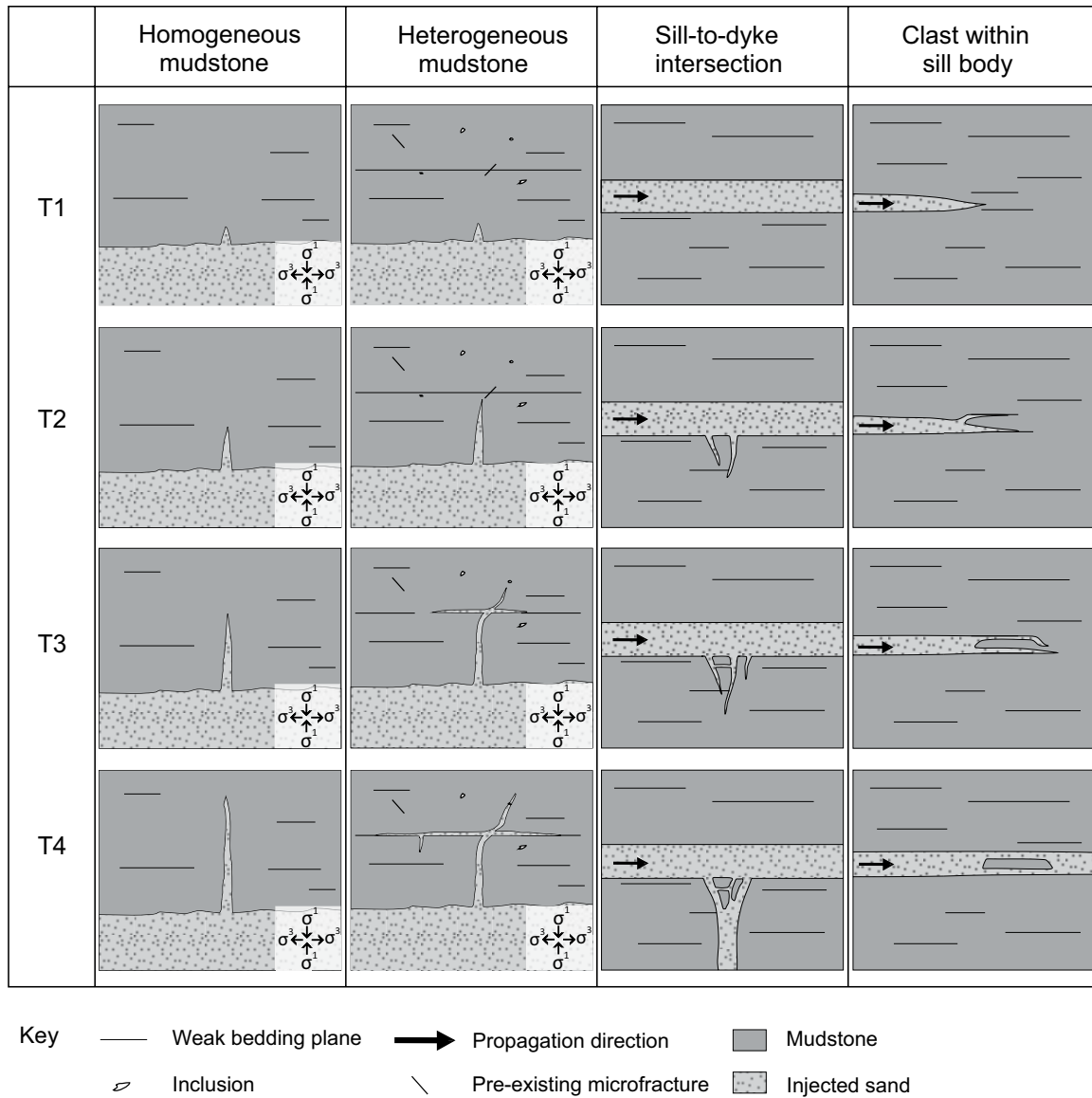
Figure 2. Temporal development (time steps T1–T4) of injectite fractures, showing simple fracture propagation in homogeneous and heterogeneous mudstones, fracture development at a sill-to-dike intersection and the formation of associated clasts, and the propagation of horizontal fractures leading to a large clast within a sill body.

of fracture and fluid-sediment emplacement (Woodworth, 1895). The types of structures seen on injectite margins in the Karoo Basin include smooth surfaces, blistered surfaces, plumose ridges, parallel ridges, and mudclast surfaces, all of which are observed at the Buffels River section (Fig. 4).

Smooth Surfaces

Description

Smooth surfaces occur on sills only. No structures or features are present on the sharp top or basal margins, and the sandstone is smooth and flat (Fig. 5A).

Interpretation

Sills represent injection along bedding planes within the host strata. Given that smooth, structureless surfaces are only seen on sill margins, they are interpreted here as defining prominent and therefore smooth bedding planes within the host mudstone. During injection of sills, the overlying strata are presumed to be lifted or forced upwards.

Blistered Surfaces

Description

A blistered surface is a smooth surface with small (<2 cm diameter, <1 cm high) subcircu-

lar bulges or bumps, which are referred to as blisters. The blisters are composed of sandstone, are roughly circular with subrounded to subangular margins, and can be concentrated into patches (Fig. 5B1) or occur in isolation (Fig. 5B2), and are only seen on sills. Locally, a lateral transition from smooth to blistered surfaces is observed, albeit associated with a degree of cutting upwards and downwards (Fig. 4B inset).

Interpretation

The largest blisters (2 cm diameter) are much smaller than the ellipsoid mudstone clasts (typically up to 10 cm in long-axis length and 4 cm
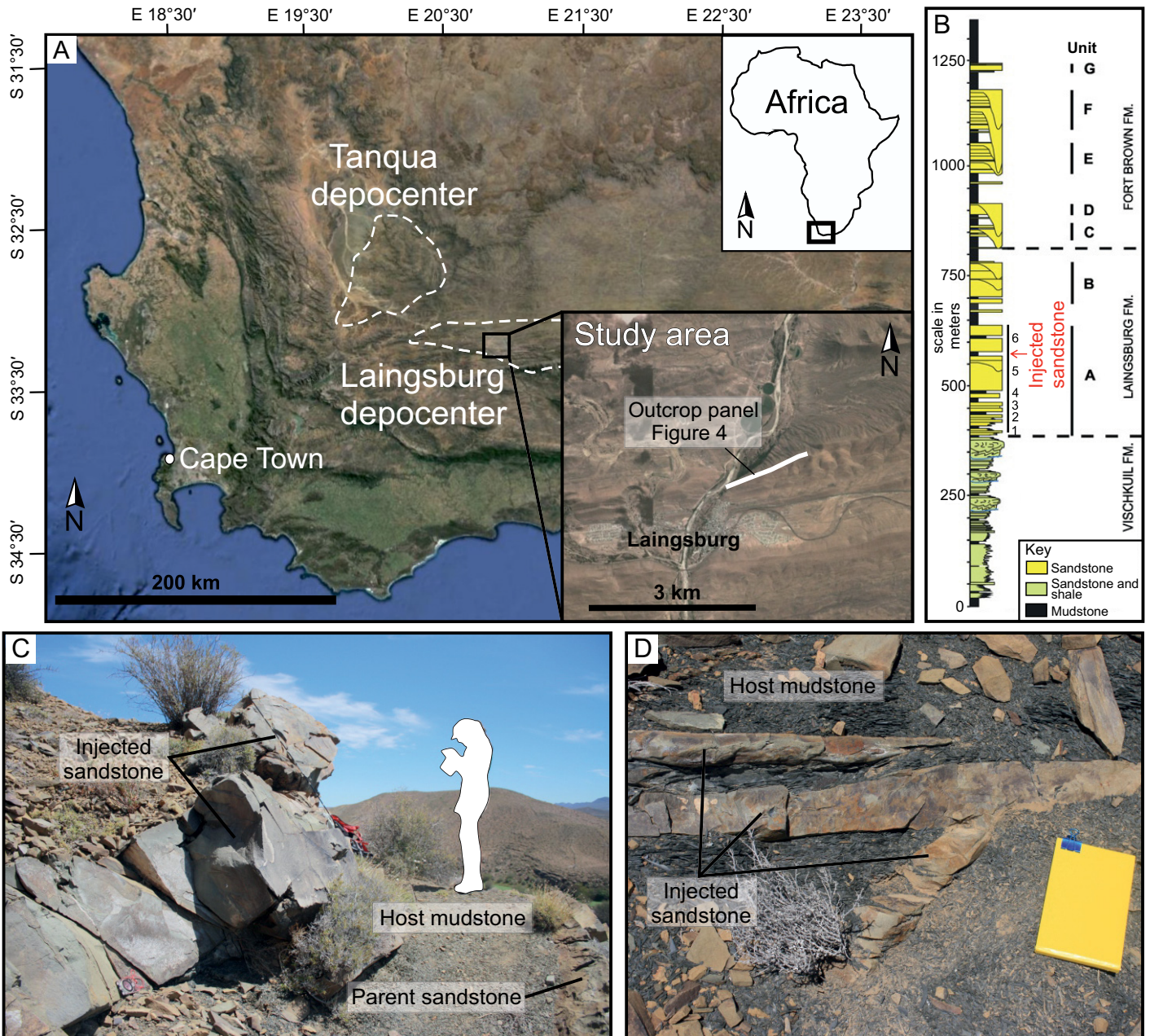
Figure 3. (A) Image of southwestern Karoo Basin with Tanqua and Laingsburg depocenters outlined and study area enlarged. Image from Google Earth. (B) Summary log of stratigraphy through Laingsburg depocenter and highlighted stratigraphic position of clastic injectites (Flint et al., 2011). Fm.—formation. (C) Typical example of a sill at outcrop. (D) Typical example of a small dike and sills at outcrop. Notebook for scale (13 × 20 cm).

diameter) that are present within the injectites, which indicates that they do not reflect primary plucking and entrainment of clasts by the injecting flow. Because blistered surfaces are only seen on sills, the blistering is related to the nature of horizontal fracturing through the host mudstones. Their presence suggests that the host mudstone is more homogeneous and lacks the prominent bedding planes associated with smooth fracture surfaces. Instead, the fracturing

of a relatively homogeneous mudstone leads to a fracture surface characterized by greater surface roughness; the blisters reflect the asperities on this surface. It is not clear why there is an abundance of subcircular blisters instead of a more random shape distribution, though it is likely influenced by the mechanisms by which the bedding planes break apart. Transitions from smooth to blistered surfaces (Fig. 4B inset) may represent spatial changes in the rela-

tive heterogeneity of the mudstone as the fractures propagate laterally and cut up and down stratigraphy.

Plumose Ridges

Description

All plumose features are observed on the margins of dikes and consist of fan-like features that range in scale from 20 to 100 cm in width with
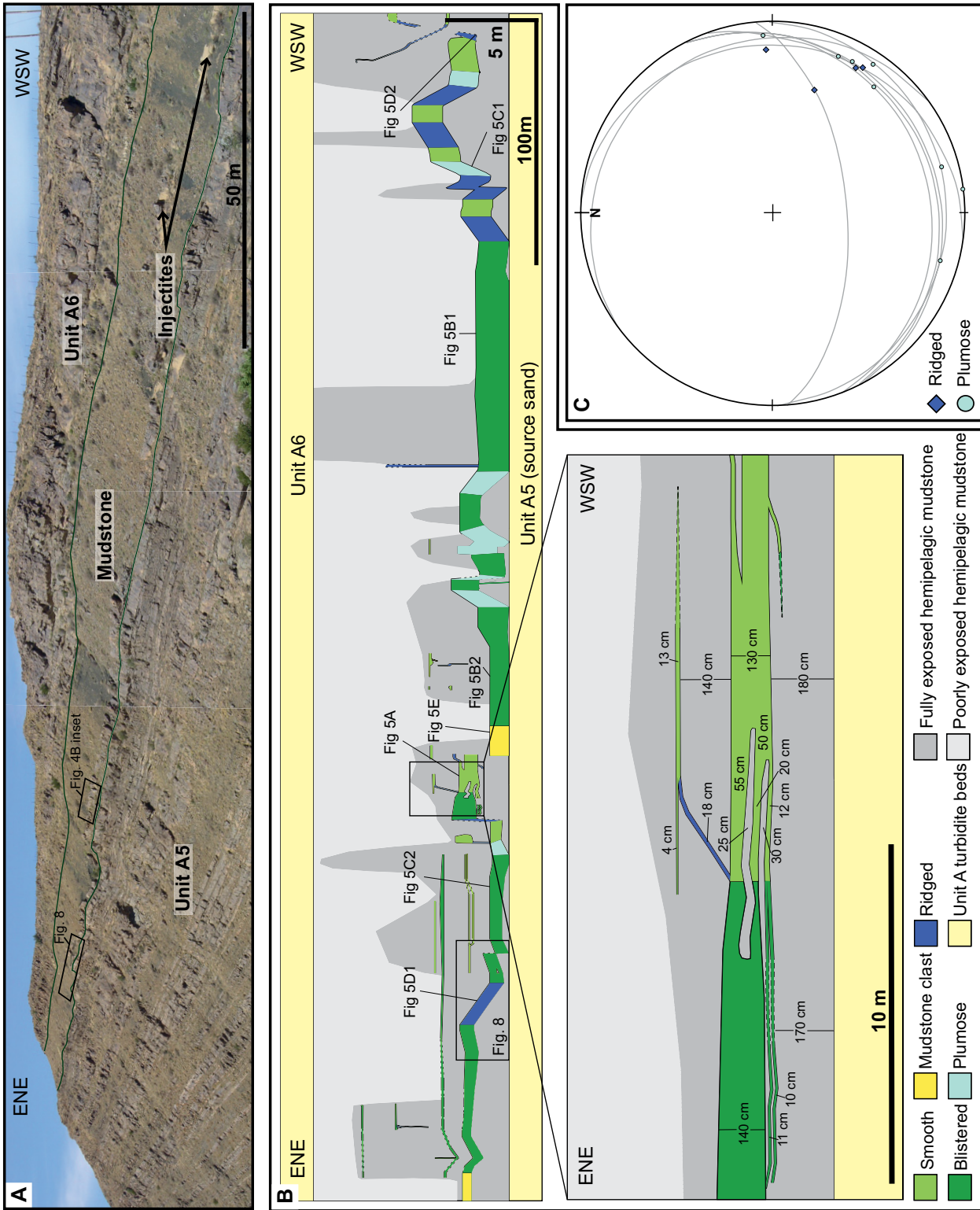
Figure 4. (A) Outcrop photo panel highlighting injectites in lobe complexes A5 and A6. (B) Panel used to correlate injectites showing the distribution of margin structures. Vertical exaggeration is 7.5. The inset shows the detailed distribution of injectites, with thicknesses and the distribution of margin structures. (C) Stereonet with restored dikes and plumose fracture and parallel ridge propagation data. Lineations are restored orientation of ridges and plumose fractures. Using the hackles (ridges) and fanning direction (plumose), the overall propagation direction was determined to be to the north and west, consequently there is a component of propagation from left to right in the figure, and another component coming out of the page toward the viewer.
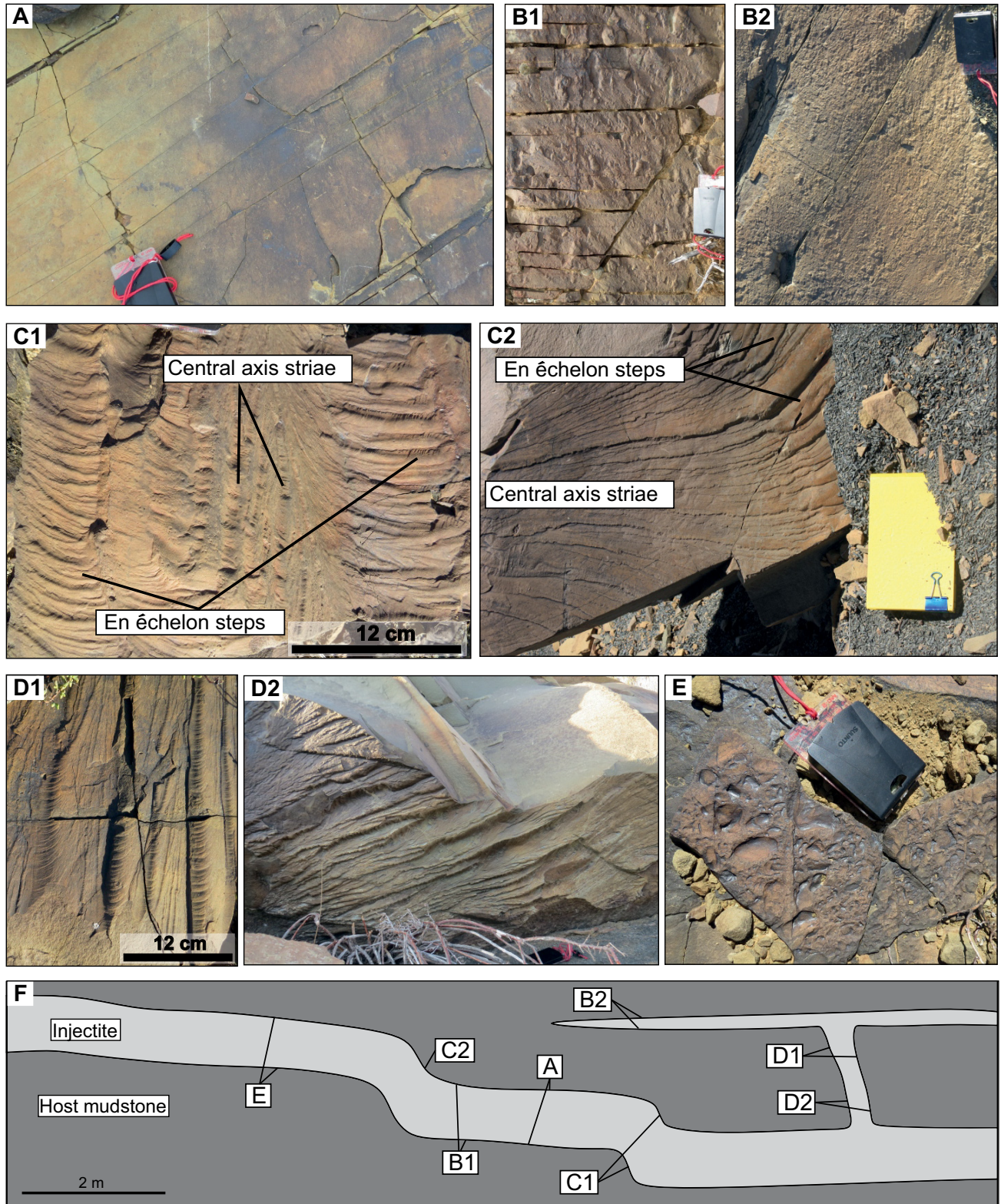
Figure 5. Representative photographs depicting typical margin structures associated with clastic injectites in the Karoo Basin, South Africa. (A) Smooth, structureless surface. Compass for scale (11 × 6 cm). (B1 and B2) Blistered surfaces, B1 showing the largest typical blisters and B2 the smallest. (C1 and C2) Two very different styles of plumose fracture, all indicating fracture direction. (D1 and D2) Parallel ridges, all on subvertical injectites and with secondary hackle marks superimposed. Notebook for scale (13 × 20 cm) (E) Margin surface where mudstone clasts have been eroded out; clasts are up to several centimeters in diameter and are in some cases rounded. (F) Cartoon of a typical cross-section through injectite with positions of margin photos A–E in relation to injectite geometry.

an angle of spread up to 180° and with relief of up to 2 cm (Fig. 5C). The main elements of the fan-like features are parallel striae down the center of the feature, diverging striae that increase in relief away from the central axis, and en echelon segments at the fringes of diverging striae. Commonly, en echelon structures on the fringes of plumose features display superimposed plumose markings on their surfaces. At the outer edge or fringe of these plumes, ridges form a step-like morphology of higher relief and a rougher texture commonly perpendicular to, or at an acute angle to, the parallel axial ridges. Restored orientation data collected for the azimuth of plumose ridges indicates a range from 265° to 015° (Fig. 4C).

Interpretation

We consider these features as an indication of the initial opening of a fracture during injection. Plumose patterns are a morphology found along fractures formed through mode I opening of homogeneous rock (e.g., Müller and Dahm, 2000; Fossen, 2010), and it has long been recognized that they provide an indication of unidirectional propagation direction (Lutton, 1970) parallel with axial striae and in the direction of plume opening and spreading (Fig. 6). As plumose patterns are only observed on the margins of dikes, they are interpreted to form through fracturing and breaking apart of host mudstone itself, and the pattern left is a cast of this fracturing. Restored propagation data indicate injection direction dominantly ranging between north and west (Fig. 4).

Ridged Margins

Description

Ridges are parallel, have up to 4 cm relief, and nearly always have a secondary set of asymmetric orthogonal ridges or hackle marks superimposed down one side that fan outwards (Fig. 5D1). Outcrop exposure allows for a maximum measured length of 1 m, with ridges always observed together in sets. They are found on the margins of dikes, and where both margins are exposed, the ridges are parallel. Typically, the crestlines of the ridges are oblique, up to 60°, to host strata bedding planes, and restored lineations are oriented 267°–303° (Fig. 4C).

Interpretation

The ridged texture on dike margins has previously been attributed to the fracturing of mudstone during forcible injection, supported by the "jigsaw"-like nature of both margins (Kane, 2010). Fracture propagation direction would have been along strike of the ridge crests (Hull, 1996), however this only offers a bidirectional
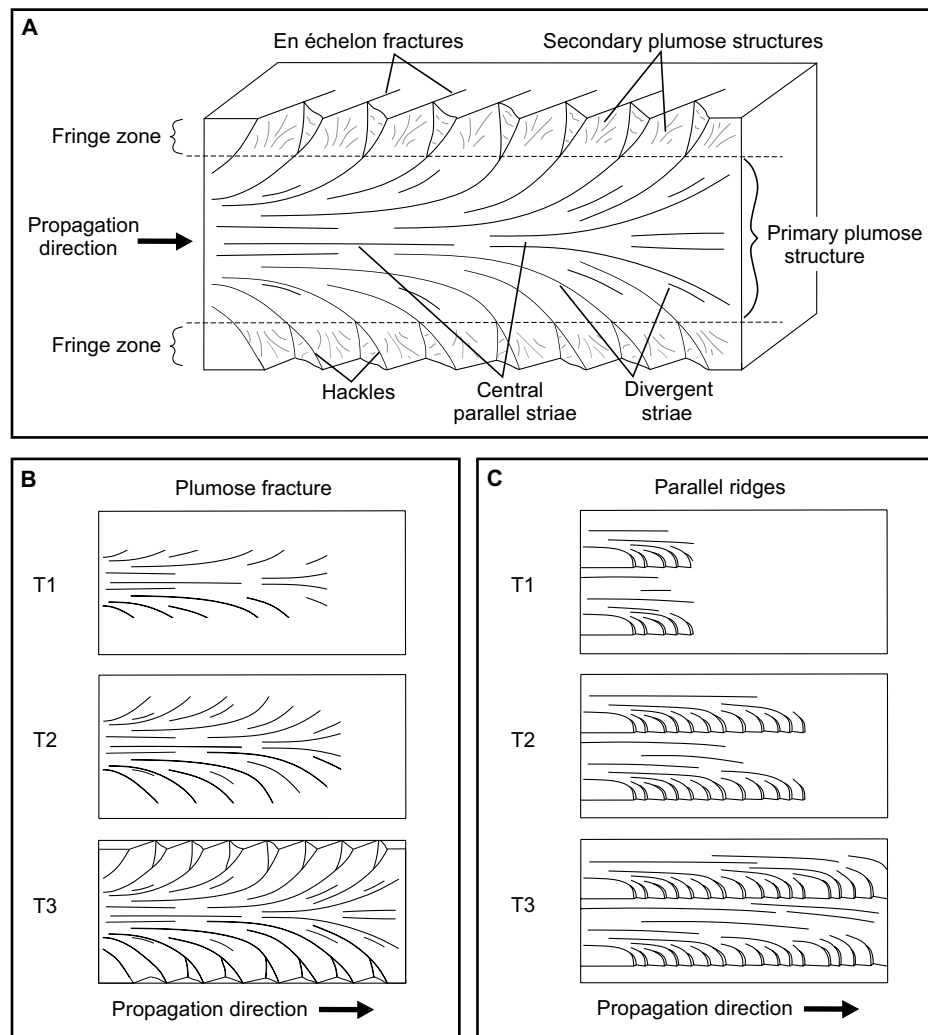
Figure 6. (A) Schematic block diagram depicting joint faces and features on a plumose fracture (adapted from Fossen, 2010). (B) Three time phases depicting formation of a single plumose fracture. (C) Three time phases depicting formation of parallel ridges with hackles.

constraint. The superimposed secondary ridges or marks, which are interpreted as hackles, indicate unidirectional propagation in the direction of fanning or toward the steep side of individual hackles (Hodgson, 1961; Lutton, 1970; Pollard et al., 1982) (Fig. 6C). Figure 4C shows this propagation direction to be between west and northwest along the Buffels River outcrop.

Mudstone Clasts

Description

Mudstone clasts are observed associated with clastic intrusion in several different ways: (1) at sill-dike intersections, (2) within sills, and (3) concentrated at sill margins.

Sill-dike intersection. Where dikes are fed by sills, angular mudstone clasts up to 20 cm in diameter are commonly present. Laminations within the mudstone clasts follow the character and orientation of laminations in the host mudstone (Fig. 7A). This is seen in intrusions >10 cm in thickness.

In sills. Mudstone clasts are also present within the body of sills, in patches up to 2 m across with the biggest clasts reaching 1 m in diameter (Fig. 7B). The clasts can themselves host minor sandstone injectites. The thickness of the sand remains continuous around the clasts.

At sill margins. Sill margins show areas up to 5 m² concentrated in mudstone clasts on both the upper and basal surfaces. Individual clasts are up to 10 cm along the long axis (of an ellipsoid pebble) and range from angular to rounded in cross-sectional shape (Fig. 5E). The largest clasts are associated with the thickest sills (>1 m thick) whereas sills <30 cm thick commonly only exhibit mudstone clasts <6 cm in length. Other

Figure 7. (A) Sill-to-dike transition zone, showing an area of in situ clasts at the sill-dike junction. Arrow represents injectite propagation direction. Notebook (13 × 20 cm) for scale. (B) Sill with an in situ mud clast >1 m in length; compass clinometer for scale. Figure 2 shows schematic views of the temporal development of these features.

than this broad correlation between sill thickness and mudstone clast size, no sorting of clasts by size or shape has been observed, and no imbrication of clasts is apparent (Fig. 5E) though the *a* and *b* axes are aligned parallel to sill margins.

Interpretation

It is widely assumed that mudstone clasts within clastic intrusions are sourced from the host strata, plucked at dike margins and incorporated into the flow of fluidized sand (Chough and Chun, 1988; Diggs, 2007; Hamberg et al., 2007; Hubbard et al., 2007). Where mudstone clasts are observed in sills, commonly toward the margins, it has been interpreted that the clasts were ripped up or ripped down from the host lithology and incorporated into the flow (e.g., Macdonald and Flecker, 2007). However, the absence of surfaces with evidence for plucking of large clasts suggests that their production was not directly associated with erosion by the sills during injection.

Sill-dike intersection. An alternative source of mudstone clasts is the complex zone of brecciation and injection immediately adjacent to the connection between sills and dikes (Fig. 7A). This in situ brecciation of the host rock through hydraulic fracturing (e.g., Duranti and Hurst, 2004) creates clasts that either remain in situ where the primary lamination can be followed across clasts (Fig. 2, sill-to-dike intersection) or are entrained into the flow of fluidized sand.

In sills. As with sill-dike intersections, it is most likely that clasts within sills are in situ, as laminations within clasts are parallel with those of the host stratigraphy (cf. Newsom, 1903). The thickness of the sill itself remains constant where these clasts are present (Fig. 7B) suggesting that the injecting flow was funneled around or through conduits above and below these clasts, leaving them in situ (Fig. 2, clast within sill body).

At sill margins. The occurrence of mudstone clasts predominantly along injectite margins is suggestive of high-concentration flow with minimal mixing because flow concentration must have been high enough to support the clasts and enable deposition along the top margins of sills as well as deposition on the base. The subangular nature of the clasts implies low erosion and abrasion during transport and deposition. An obvious source for these clasts is the zone of brecciation at sill-dike intersections. Erosion of injectite walls during injection is ruled out due to the complete lack of any erosive features both on sills and dikes. Blistered surfaces have dimples, bumps, and bulges with maximum diameters of 2 cm, whereas the largest clasts are up to 10 cm in long-axis length and 4 cm in diameter (see Appendix Table A1). The difference in size between blisters and clasts suggests that the blistered surfaces were not the source of the clasts.

Stepped Sills

Description

Step-ramp-step geometries are generally up to 1 m in height and crosscut stratigraphy at between 10° and 70°. Structures seen on step margins are either plumose (most common) or parallel ridges. Figure 4B shows an example of a sheet sill stepping through stratigraphy multiple times over 500 m of outcrop.

Interpretation

Steps refer to the particular geometry of an injectite, which is also recognized in igneous intrusions (e.g., Schofield et al., 2012) (Fig. 8A). As the intrusion geometry represents the fracture mechanics of the host strata and not the injecting fluid, the same interpretation of step formation can be applied to clastic dikes and sills. Similar step features have previously been identified in clastic intrusions (Vétel and Cartwright, 2010). Steps occur when intrusion tips propagating through brittle strata become slightly offset (Schofield et al., 2012), resulting in en echelon fracture propagation with individual steps increasing in height or offset in the direction of fracture growth (Pollard et al., 1975; Schofield et al., 2012). Therefore the exposure
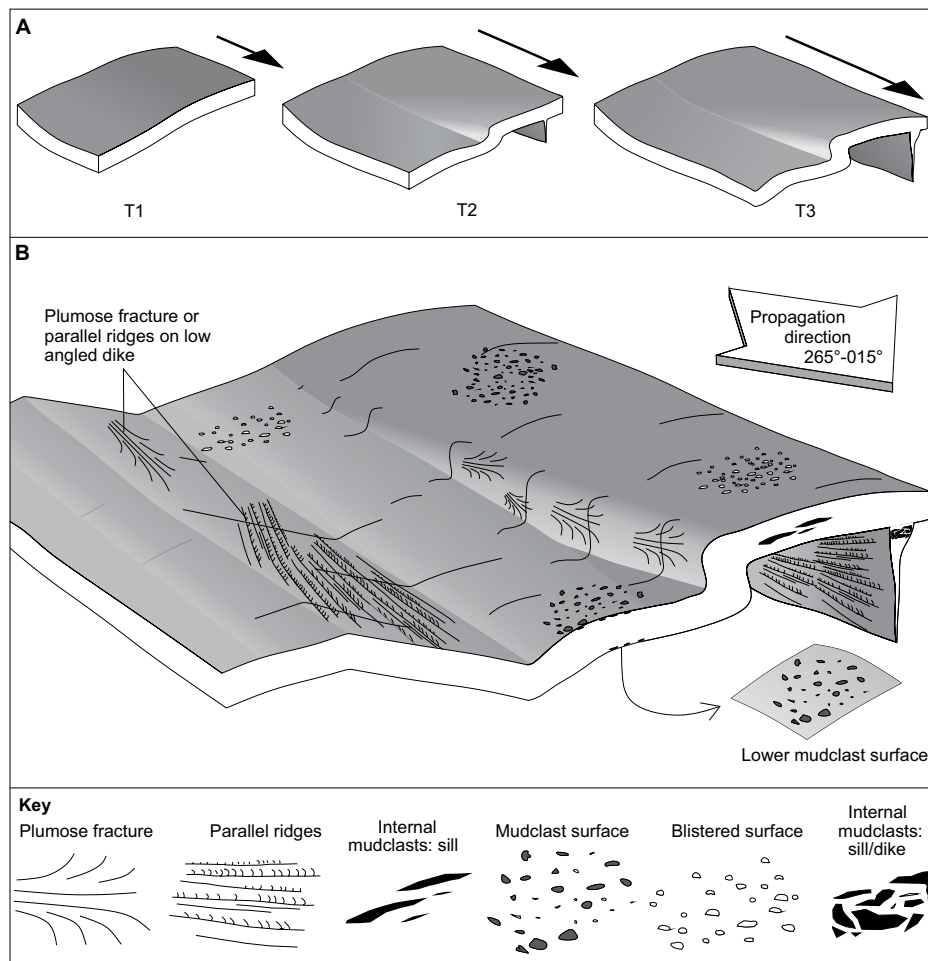
Figure 8. (A) Three time phases showing the formation of a stepped sill as an injectite propagates. Arrow indicates propagation direction. (B) Schematic diagram showing spatial distribution of internal and external injectite structures.

of steps at outcrop, as well as at a larger scale in seismic data, could be used to identify initial fracture and therefore propagation direction (Figs. 4B and 8A).

Summary of Spatial Distribution of Injectite Margin Structures

These differing margin structures each occur in spatial positions specific to the injectite geometry. The array of margin structures is synthesized in Figure 8; mudstone clasts and smooth and blistered surfaces are found on margins of sills where injection is parallel with host strata, while in contrast, ridged and plumose margins are associated with dikes and where injection is discordant with host strata (Figs. 5F and 8B). Figure 8 also illustrates the relative positions of mudstone clasts within injectites: those within sill bodies and those at the sill-dike intersection. In summary, each

of the structures described in the previous sections only occur in specific localities relating to injectite architecture and can be categorized on this basis.

DISCUSSION

Previous work on structures on injectite margins has identified both those of a primary nature associated with initial fracturing and features related to later erosion by flows associated with the injection process (Peterson, 1968; Taylor, 1982; Surlyk and Noe-Nygaard, 2001; Hillier and Cosgrove, 2002; Hurst et al., 2005; Diggs, 2007; Hubbard et al., 2007; Kane, 2010). In the present study, many of these margin structures show strong similarities with fracture-related features formed in previously documented settings and experimental research (plumose, parallel ridges, steps opening in direction of propagation) (Hodgson, 1961; Lutton, 1970; Müller

and Dahm, 2000). In addition, the dikes and sills show no evidence for erosion along their margins, with many sill-dike intersection regions showing the only evidence for host lithology entrainment. Intricate features such as the plumose structures on dikes and steps are preserved in a pristine state, while the sill margins are either smooth or associated with structures that are far smaller than the clasts that are observed within the injectite. Consequently, there is strong evidence that these injectite margin structures are primary features caused directly by the fracturing process, and that the injectites essentially serve as casts of the fracture surface. This allows us to use these features to determine propagation direction, depth of emplacement relative to the tensile strength of the host mudstone, and processes of the injecting flows.

Determining Injection Propagation Direction Using Margin Structures

Plumose Pattern

Plumose patterns are interpreted to reflect the way in which the host mudrock initially fractured immediately prior to injection of fluids and sand, with the direction of fracture, and therefore injection, parallel with the plume axis (Fossen, 2010). Generally, a fracture in a brittle rock propagates along a plane perpendicular to the axis of minimum compression, and the fracture itself forms under tension (Fig. 1, mode I) (Pollard et al., 1982; Lorenz et al., 1991; Fossen, 2010). However, if the principal stress axis rotates as plumose fractures form, causing fracture direction to change, then shear fracturing (mode III) will occur at the newly oriented fracture front in order to adjust to the new stress state (Fig. 1; Sommer, 1969). Therefore, if the propagation at the tip of the main fracture is occurring under a tensional regime, then as the ridges that form the plumose fracture diverge, the fracture propagation direction is no longer perpendicular to the axis of minimum compression. To compensate, fracture by shearing takes place, which leads to the formation of en echelon steps at its tip (Pollard et al., 1982), oriented oblique to the parent fracture plane (Bahat, 1986) (Fig. 6). En echelon structures always form in a specific orientation related to the overall stress regime and therefore, at a given outcrop, will likely all have the same orientation. Orientation data from the sheet injection and connected dikes of the Buffels River outcrop indicate a northwest propagation direction (Figs. 4B, 4C, and 8B).

Where outcrop allows for injectites to be observed in three dimensions, multiple sets of plumose fractures are observed along steps. In these cases, multiple plumose fractures are indicative of a broad yet definitive propagation direc-

tion, as synthesized in Figures 6 and 8B. Experimental work by Sharon et al. (1995) has related velocity of fracture propagation through multiple fractures with a constant overall energy state. From initial fracture, velocity of propagation increases until the critical velocity for the onset of branching (v_c) is reached. It is at this point that the en echelon–style fringe of the plumose fracture initiates (Sharon et al., 1995; Bahat, 2001). Fracture propagation velocity decreases as the relief on the fracture plane increases due to the enlargement in fracture area (Müller and Dahm, 2000; Bahat, 2001; Chemenda et al., 2011). In the case of plumose fractures, this would be from the central plumose structure to the en echelon fringes. Energy that was solely being used to propagate the parent fracture is now subdivided between parent and daughter cracks (central axis striae and en echelon cracks respectively). Less energy is available for the fracture to continue propagating, and therefore overall propagation velocity slows (Sharon et al., 1995). The daughter en echelon cracks have a restricted lifetime, and once they stop, all of the energy is then returned to forward propagation and another plumose fracture forms (Sharon et al., 1995). These extensional fractures grow in pulses, with each propagation pulse ending by slowing down or completely stopping until enough energy has built up to initiate the next pulse and plumose fracture (Fossen, 2010). At outcrop, therefore, it is possible to gain an understanding of local stress within the rock at the time of fracture from a small group of plumose patterns, and it is feasible to estimate a more widespread stress regime from collecting orientation data over a large area.

Parallel Ridges

Kane (2010) suggested that an observed "ropey" texture on injectite margins is a result of the splitting apart of the host sediment, as the feature is commonly parallel on opposite margins. Second-order hackle marks (Fig. 6C) indicate unidirectional fracture propagation, and therefore injection direction can be determined through observation of this particular structure using similar criteria to plumose fractures (Figs. 5D1 and 6A). This is supported where injection direction is constrained from plumose fractures and steps. On outcrop, ridges are continuous as far as observation allows, and therefore unlike pulsed plumose fracture propagation, it is likely that these occur during quasi-constant fracture propagation.

Estimating Injection Depth

Where injectite complexes reach the seabed and extrude sand, it is possible to give a minimum depth of injection from lowermost intrusions up

to extrusions (Surlyk and Noe-Nygaard, 2001; Thompson et al., 2007; Ross et al., 2013, 2014). For example, the Panoche Giant Injection Complex in California has an estimated thickness of 500–750 m (Vigorito et al., 2008; Vigorito and Hurst, 2010; Scott et al., 2013). However, where clastic injectites do not reach the surface, there has been no methodology proposed for estimating the depth of intrusion. Here we show that the mode of fracture can be used for relative depth estimation. Here we also explore the possibility of extending this to estimation of true depths, and discuss why this is not presently possible.

The state of stress during burial in a tectonically quiescent basin is assumed to be confining, and therefore extensional fractures are unusual. However, natural hydraulic fractures are a form of extension in a setting with confining stresses (Phillips, 1972; Cosgrove, 2001). Clastic dikes form in extensional (tensile) fractures, which are usually typical of deformation at low differential stresses ($\sigma_1 - \sigma_3$) or confining pressures. In settings of high fluid pressure, however, low differential stress and mode I (tensile) fractures can occur at several hundreds of meters depth (Secor, 1965; Aydin, 2000; Cosgrove, 2001) with the expression or relief of these features increasing with increasing pressure (Chemenda et al., 2011). Near to the surface, mud has low tensile strength despite being cohesive, and therefore will undergo plastic deformation when stress is applied (Lowe, 1975; Nichols et al., 1994). Muds exhibit higher tensile strengths at depth, thereby enabling mode I failure in the host sediment (Jolly and Lonergan, 2002). This combination of the depth distribution of tensile strength in muds and the high fluid pressures associated with injection suggests that mode I failure will occur at considerable depths (up to hundreds of meters).

Shear failure occurs at a depth where the applied shear stress, S, is greater than four times the tensile strength of the rock, T, changing from extensional fracturing at shallower depths (Fig. 1). Plumose fractures with en echelon fringes form from mainly extensional deformation (central and divergent striae) but with a component of shear fracturing. This could place a depth range on formation of fractures and injection at or near to the bounding zone from extensional to shear stresses.

Extending this estimation of relative depth to true depth is challenging for a number of reasons. Firstly, a depth profile for the tensile strength of the host shale must be calculated. This can be achieved by: (1) calculating porosity as a function of depth for shales (e.g., Baldwin and Butler, 1985); (2) calculating the uniaxial compressive strength of shale as a function of porosity:

$$C_0 = 243.6\phi^{-0.96}, \qquad (1)$$

where C_0 is the uniaxial compressive strength and ϕ is porosity (Horsrud, 2001; Lothe et al., 2004); and finally, (3) assuming that the tensile strength is one-tenth that of the uniaxial compressive strength (Lothe et al., 2004). Thus an estimate of the profile of tensile strength, T, with depth can be calculated. Given that shear failure occurs where applied shear stress is >$4T$, then the applied stress needs to be calculated. Estimates of propagation rate in injectites range from 0.1 to 10 ms^{-1} (Bureau et al., 2014) based in part on comparison with igneous intrusions (Rubin, 1995). However, the applied stress at the tip of a paleofracture is difficult to estimate because knowledge of the processes occurring in the area immediately around the propagating fracture tip is limited and the rate of fracture propagation is hard to predict (Fineberg and Marder, 1999; Bahat et al., 2005).

Although absolute depths of injection cannot be calculated, relative depth of injection can be estimated. Based on analysis of the fracture patterns occurring at a depth where tensile strength is at least four times that of the host mudstone, it is possible to rule out shallow injection. Furthermore, injectites with margin structures indicative of this range of fracture modes are able to form at up to several hundreds of meters depth. This approach enables relative injection depth to be inferred for systems that are not connected to the surface.

Flow Processes during Injection

The nature of flow in injectites has been the subject of much debate, with arguments for both laminar flow (Dott, 1966; Peterson, 1968; Taylor, 1982; Sturkell and Ormö, 1997) and turbulent flow (Obermeier, 1998; Duranti, 2007; Hubbard et al., 2007; Scott et al., 2009) being forwarded. Scott et al. (2009, p. 575) suggested that a "spectrum of flow conditions from low-velocity viscous, hydroplastic laminar flow to high-velocity, turbulent flow probably occurs." In a more recent paper, Hurst et al. (2011, p. 239) have argued that "evidence of a turbulent flow regime during sand injection is prevalent."

The distribution of transported mud clasts at both the top and base of sills (Fig. 5E and 8B) suggests that the flow was highly concentrated, because the particles at the top were unable to settle through the sediment; similar features are also observed in other examples (see Macdonald and Flecker, 2007; Hurst et al., 2011). The mechanism for this observed segregation of mud clasts toward the wall regions of the sills is unclear, but both potential mechanisms, (1) incorporation and maintenance of particles near the edge of the flow and (2) segregation of particles within the flow, suggest high-concentration, slow-moving flows. Particles may have been incorporated near the edge of the flow, and given the short transport distances and high concentration, may not have mixed into the flow. Another possible mechanism is inertial induced lateral migration of particles toward the walls, which occurs in laminar flows (Segré and Silberberg, 1962a, 1962b). Where density differences in particles are present, less dense particles will preferentially move toward the walls (Hogg, 1994). Densities of shales at the suggested depths of hundreds of meters are likely in the region of 1900–2300 kg m^{-3} (Rieke and Chilingarian, 1974; Castagna et al., 1993), so the mud clasts will be less dense than the quartz-dominated sand grains (~2650 kg m^{-3}). Such affects have been observed experimentally for small particles, with correspondingly low particle Reynolds numbers, under laminar flow conditions (Segré and Silberberg, 1962a, 1962b; Hogg, 1994). However, it is unclear if this mechanism extends to larger low-density particles in laminar flows. Rounding of many of the mud clasts is in accordance with some transport prior to deposition, although the angularity of some clasts and the absence of evidence for local sourcing suggest that the flow was not particularly turbulent and abrasive. The preservation of delicate structures such as the pristine plumose structures also indicates that significant abrasion did not take place at fracture margins during injection emplacement. For example, there is no evidence for scratches on these features, or of features indicative of turbulent flow such as flute marks (Allen, 1982; Hurst et al., 2011). In fact, no evidence of erosion has been observed within the sills and dikes, and the main features on injectite margins are all interpreted to be a primary function of the fracture process. The absence of any evidence of abrasion or erosion further suggests that the injections were associated with high-concentration, relatively slow-moving flows.

The flow processes are further assessed through calculation of flow Reynolds numbers, Re, using the methodology of Ross et al. (2014):

$$Re = (UA\rho_{pf})/\mu_{pf}, \qquad (2)$$

where U is velocity of the injection, A is the fracture aperture, and ρ_{pf} and μ_{pf} are the pseudofluid density and viscosity respectively, with the pseudofluid being the mixture of water and fine-grained particles (Di Felice, 2010; Ross et al., 2014). The method estimates the velocity of the injected suspension, U, as being equal to or greater than the fall velocity of the largest particle (see Ross et al. [2014] for full details). Previous estimates of velocities in injectites were based on two-dimensional sections and utilized the largest observable length as the grain diameter (Scott et al., 2009; Ross et al., 2014), leading to potential errors in the calculation of velocities if particles are strongly ellipsoid (Matthews, 2007). In this field example, the way in which the ellipsoidal mud clasts weather out on surfaces enables a more accurate equivalent spherical diameter to be calculated.

The velocity calculations assume that the volumetric particle concentrations are high, because the large particles are unable to settle through the flow. However, the exact volumetric flow concentration is unknown, and therefore a range of concentrations (solid volume fractions) is considered. Solid volume fractions range from close to the highest possible value for fluidization (0.54) (Leva, 1959; Scott et al., 2009; Ross et al., 2014) down to a more conservative value of 0.4 that might not be expected to fully support the large particles at the upper margins of sills. These calculations demonstrate that flow Reynolds numbers for many of the dikes and sills are either in the laminar flow regime, Re < ~2300 (for fractures, injectites and pipes; Singhal and Gupta, 1999; Faisst and Eckhardt, 2004; Scott et al., 2009; Post, 2011), or in the transitional flow regime, ~2300 < Re < ~4000 (Faules and Boyes, 2009; Munson et al., 2012) (see Table 1). If, as argued here, solid volume fractions are close to the highest grain concentration possible for fluidization (0.54), then almost all of the injectites likely formed under laminar conditions (up to 1.1 m thick), with the remainder exhibiting transitional flows (up to the maximum observed thicknesses of 1.3 m) (Table 1). If lower solid volume fractions were prevalent, then flows were likely laminar or in the transitional regime for the vast majority of sills (up to 0.8 m thick) for solid volume fractions of 0.47, and even at solid volume fractions as low as 0.4, sills and dikes up to 0.35 m thick are predicted to be laminar or transitional (Table 1).

Predicting Laminar and Turbulent Injection Flow Processes and Products

Evidence in support of turbulent flows (Fig. 9A) in injectites comes from flow Reynolds number calculations based on fall velocities of large clasts (Duranti and Hurst, 2004; Scott et al., 2009; Sherry et al., 2012; Ross et al., 2014), erosional margins and the formation of features such as scours (Hubbard et al., 2007; Vigorito et al., 2008; Vigorito and Hurst, 2010; Scott et al., 2013), and normal grading (Obermeier, 1998; Hubbard et al., 2007; Ross et al., 2014). Internal laminations have been inter-

TABLE 1. CALCULATED FLOW REYNOLDS NUMBERS

Aperture (m)	Reynolds number, grain concentration 54%	Reynolds number, grain concentration 47%	Reynolds number, grain concentration 40%
0.1	199.37	490.03	1030.01
0.2	398.74	980.06	2060.02
0.3	598.10	1470.09	3090.03
0.4	797.47	1960.12	4120.04
0.5	996.84	2450.16	5150.05
0.6	1196.21	2940.19	6180.06
0.7	1395.57	3430.22	7210.07
0.8	1594.94	3920.25	8240.08
0.9	1794.31	4410.28	9270.09
1.0	1993.68	4900.31	10,300.10
1.1	2193.04	5390.34	11,330.10
1.2	2392.41	5880.37	12,360.11
1.3	2591.78	6370.41	13,390.12

Note: Flow Reynolds numbers are for grain concentrations of 54%, 47%, and 40% in sill apertures ranging from 0.1 m to 1.3 m. All calculations are for an ellipsoid mudstone pebble 10 cm along the longest axis.

preted as the product of both laminar (Dott, 1966) and turbulent flows (Hurst et al. [2011] citing Lowe's [1975] work), and their observation in terms of flow process remains equivocal (Hurst et al., 2011). The examples of interpreted turbulent flow described in the references above are either from injectite systems that reached the paleosurface or are of unknown vertical extent (Hubbard et al., 2007). In contrast, systems interpreted to exhibit laminar flows (Fig. 9B) lack evidence for grading or scouring and contain abruptly tapering sills and dikes, suggesting that they formed at depth and without a surface connection (Taylor, 1982). The present study exhibits the same structures and geometric relationships as the work of Taylor (1982) but enables quantification of flow conditions for the first time, demonstrating that small dikes and sills at depth (up to a few tens of centimeters in thickness) almost certainly form under laminar

conditions and suggesting that even relatively large sills (on the order of 1 m) may well be formed under laminar conditions.

When fractures occur at depth without an open connection to the surface, then there is a limited capacity for flow dilution, with liquid and particulate components moving together from high to low pressure, thereby encouraging high-concentration flows. Such high-concentration flows are far less likely to exhibit turbulent conditions because flow viscosity varies strongly (by orders of magnitude) with flow concentration (e.g., Krieger and Dougherty, 1959). As a consequence, the viscous term in the Reynolds equation (Equation 2) is likely dominant unless the cross-sectional dimensions (fracture aperture) of injectites become large. In contrast, once connection to the surface occurs, a greater fraction of carrier fluid to particles can be accommodated, enabling highly turbulent and lower-concentration flows to form. Essentially, overpressured water is able to escape to the surface, and in so doing, carry particles with it. Observations of active sand volcanoes in nature and in the laboratory demonstrate that the resulting extrusions are not high-concentration granular flows, but are lower-concentration systems (Ross et al., 2011; Quigley et al., 2013).

Figure 9. Recognition criteria for distinguishing between laminar and turbulent flow in clastic injectites. (A) Injectite architecture and features expected as a product of turbulent flow during clastic injection. Grading, both normal and reversed, within injectites is typically related to turbulent flow and is most likely a function of parent sand composition and preferential fluidization of grain sizes. Erosive or groove marks on the margins of sills or dikes and rounded clasts throughout the deposit also suggest turbulent flow. Mud clasts within the injected sandstone are in some cases bounded by or injected by one-grain-thick sand-filled fissures. Dikes forming extensive vertical conduits, potentially forming pipes and subsequently extrudites, are also an indicator of turbulent flow. (B) Schematic diagram of typical injectite architecture and structures associated with laminar flow.
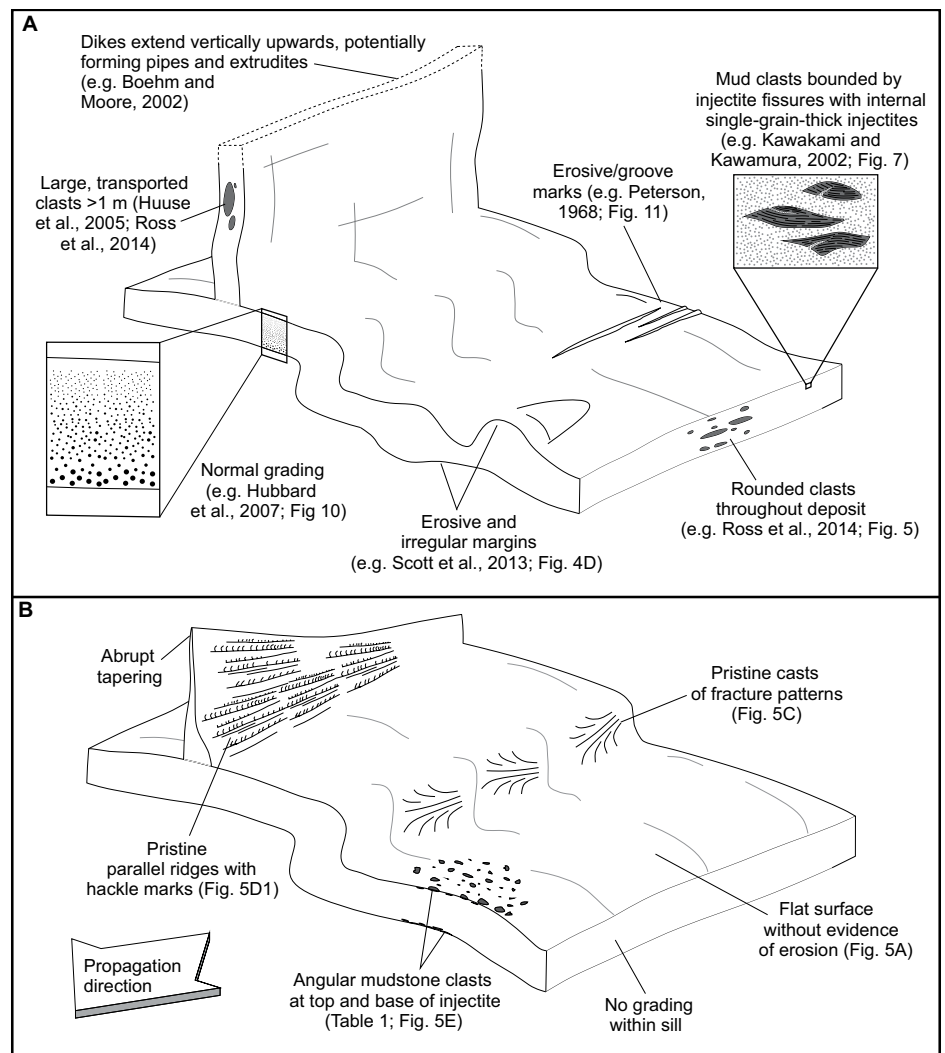
Given these parameters, it is possible to envisage three broad categories of flow during injection: (1) flows that are connected to the surface where flows are relatively low concentration and highly turbulent; (2) large-scale injectites that do not have a connection to the surface and that will exhibit high-concentration turbulent flows; and (3) flows with no connection to the surface and with relatively small cross-sectional dimensions (tens of centimeters) where flows will be highly concentrated and laminar. Correspondingly, the products of these flows will be different, with structures such as grading and erosional scours prevalent in low-concentration open conduits, while such features will be lacking in smaller-scale laminar injectites in closed conduits. The degree to which larger-scale closed systems might exhibit erosive structures and grading is largely unknown.

CONCLUSIONS

The clastic injectites studied herein have led to a classification for common structures seen on the margins of sills and dikes as well as common assemblages of clasts within the injectites. Using plumose marks, parallel ridges, and steps within sills, it is possible to establish initial fracture propagation directions and therefore overall injection direction of dikes and sills. The use of these margin structures also makes it possible to estimate relative injection depth where applied stress exceeds four times the tensile strength of the host rock. Furthermore, flow estimates for clastic injections suggest that laminar conditions prevail in dikes up to tens of centimeters thick and in sills up to a meter thick if, as the evidence suggests, particle concentrations were close to the limit of fluidization (solid volume fraction of 0.54). This study provides a new set of criteria for determining flow direction and depth of emplacement within clastic injectites, as well as demonstrating high-concentration laminar flow during injection. The existing debate on the nature of flow, laminar versus turbulent, during injection is addressed here in terms of whether the injection occurred in an open (linked to surface) or closed system.

TABLE A1. CALCULATION PARAMETER VALUES

Parameter	Value(s)
g (m s^{-2})	9.81
ρ_S (kg m^{-3})	2650
ρ_L (kg m^{-3})	2100
ρ_f (kg m^{-3})	1000
φ	0.54–0.4
φ_S	0.53–0.39
φ_L	0.01
$C_{D,O}$	1.4
D_p, large particle (m)	0.071
D_s, large particle (m)	0.044
μ_f (Pa s)	0.00106
A (m)	0.1–1.3
ρ_{pf} (kg m^{-3})	0.0087–0.028
μ_{pf} (Pa s)	0.0043–0.0091
n	2.25

Note: Table A1 shows the parameters used in order to calculate flow velocities and flow Reynolds numbers for clastic injections in the Karoo Basin (see Table 1). Where parameters listed are a range, the numbers represented are for grain concentrations 54%–40% (solid volume fractions of 0.54–0.4). The methodology of Ross et al., (2014) was implemented here. In Table A1, g is acceleration due to gravity (m s^{-2}), ρ is density (kg m^{-3}), φ is the solid volume fraction, $C_{D,O}$ is the drag coefficient for a solitary particle in relative motion with an infinite fluid (non-dimensional), D_p is the diameter of a circle of the same area as the projected profile of the particle in its most stable orientation (m), D_s is clast diameter as the diameter of a sphere with the same volume as the particle (m), μ is kinematic viscosity (Pa s), A is fracture aperture (m), and n is an exponent that is a function of particle shape. Subscripts are as follows: S—small particle; L—large particle; f—fluid; pf—psuedo fluid.

REFERENCES CITED

Allen, J.R.L., 1982, Sedimentary Structures: Their Character and Physical Basis, Volume II: Elsevier, Amsterdam, Developments in Sedimentology, v. 30B, 663 p.

Allen, J.R.L., 2001, Principles of Physical Sedimentology (reprint of first edition [1985], with corrections): Caldwell, New Jersey, Blackburn Press, 272 p.

Aubertin, M., and Simon, R., 1997, A damage initiation criterion for low porosity rocks: International Journal of Rock Mechanics and Mining Sciences, v. 34, p. 17. e1–17.e15, doi:10.1016/S1365-1609(97)00145-7.

Aydin, A., 2000, Fractures, faults, and hydrocarbon entrapment, migration and flow: Marine and Petroleum Geology, v. 17, p. 797–814, doi:10.1016/S0264-8172 (00)00020-9.

Bahat, D., 1986, Criteria for the differentiation of en echelons and hackles in fractured rocks: Tectonophysics, v. 121, p. 197–206, doi:10.1016/0040-1951(86)90043-0.

Bahat, D., 2001, Changes of crack velocities at the transition from the parent joint through the en échelon fringe to a secondary mirror plane: Journal of Structural Geology, v. 23, p. 1215–1221, doi:10.1016/S0191-8141 (00)00187-5.

Bahat, D., Rabinovitch, A., and Frid, V., 2005, Tensile Fracturing in Rocks: Berlin, Springer-Verlag, 570 p.

Baldwin, B., and Butler, C.O., 1985, Compaction curves: American Association of Petroleum Geologists Bulletin, v. 69, p. 622–626.

Ben-Zion, Y., and Morrissey, J., 1995, A simple re-derivation of logarithmic disordering of a dynamic planar crack due to small random heterogeneities: Journal of the Mechanics and Physics of Solids, v. 43, p. 1363–1368, doi:10.1016/0022-5096(95)00042-H.

Boehm, A., and Moore, J.C., 2002, Fluidized sandstone intrusions as an indicator of paleostress orientation, Santa Cruz, California: Geofluids, v. 2, p. 147–161, doi:10.1046/j.1468-8123.2002.00026.x.

Bureau, D., Mourges, R., and Cartwright, J., 2014, Use of a new artificial cohesive material for physical modelling: Application to sandstone intrusions and associated fracture networks: Journal of Structural Geology, v. 66, p. 223–236, doi:10.1016/j.jsg.2014.05.024.

Cartwright, J., James, D., Huuse, M., Vetel, W., and Hurst, A., 2008, The geometry and emplacement of conical sandstone intrusions: Journal of Structural Geology, v. 30, p. 854–867, doi:10.1016/j.jsg.2008.03.012.

Castagna, J.P., Batzle, M.L., and Kan, T.K., 1993, Rock physics—The link between rock properties and AVO response, *in* Castagna, J.P., and Backus, M.M., eds., Offset-Dependent Reflectivity—Theory and Practice of AVO Analysis: Society of Exploration Geophysicists Investigations in Geophysics 8, p. 124–157.

Charlez, P.A., 1991, Rock Mechanics, Volume 1: Theoretical Fundamentals: Paris, Editions Technip, 360 p.

Chemenda, A.I., Nguyen, S.H., Petit, J.P., and Ambre, J., 2011, Experimental evidences of transition from mode I cracking to dilatancy banding: Comptes Rendus Mécanique, v. 339, p. 219–225, doi:10.1016/j.crme .2011.01.002.

Chough, S.K., and Chun, S.S., 1988, Intrastratal rip-down-clasts, Late Cretaceous Uhangri Formation, southwest Korea: Journal of Sedimentary Petrology, v. 58, p. 530–533.

Cosgrove, J.W., 1995, The expression of hydraulic fracturing in rocks and sediments, *in* Ameen, M.S., ed., Fractography: Fracture Topography as a Tool in Fracture Mechanics and Stress Analysis: Geological Society of London Special Publication 92, p. 187–196.

Cosgrove, J.W., 2001, Hydraulic fracturing during the formation and deformation of a basin: A factor in the dewatering of low-permeability sediments: American Association of Petroleum Geologists Bulletin, v. 85, p. 737–748.

Davies, R.J., Huuse, M., Hirst, P., Cartwright, J., and Yang, Y., 2006, Giant clastic intrusions primed by silica diagenesis: Geology, v. 34, p. 917–920, doi:10.1130 /G22937A.1.

Delaney, P.T., Pollard, D.D., Ziony, J.I., and McKee, E.H., 1986, Field relations between dikes and joints: Emplacement processes and paleostress analysis: Journal of Geophysical Research, v. 91, p. 4920–4938, doi:10 .1029/JB091iB05p04920.

Di Celma, C.N., Brunt, R.L., Hodgson, D.M., Flint, S.S., and Kavanagh, J.P., 2011, Spatial and temporal evolution of a Permian submarine slope channel–levee system, Karoo Basin, South Africa: Journal of Sedimentary Research, v. 81, p. 579–599, doi:10.2110/jsr.2011.49.

Di Felice, R., 2010, Liquid–solid suspension theory with reference to possible applications in geology: Basin Research, v. 22, p. 591–602.

Diggs, T.N., 2007, An outcrop study of clastic injection structures in the Carboniferous Tesnus Formation, Marathon basin, Trans-Pecos Texas, *in* Hurst, A., and Cartwright, J. eds., Sand Injectites: Implications for Hydrocarbon Exploration and Production: American Association of Petroleum Geologists Memoir 87, p. 209–219.

Diller, J.S., 1890, Sandstone dikes: Geological Society of America Bulletin, v. 1, p. 411–442, doi:10.1130/GSAB -1-411.

Dixon, R.J., Schofield, K., Anderton, R., Renolds, A.D., Alexander, R.W.S., Williams, M.C., and Davies, K.G., 1995, Sandstone diapirism and clastic intrusion in the Tertiary submarine fans of the Bruce-Beryl Embayment, Quadrant 9, UKCS, *in* Hartley, A.J., and Prosser, D.J., eds., Characterization of Deep Marine Clastic Systems: Geological Society of London Special Publication 94, p. 77–94.

Dott, R.H., 1966, Cohesion and flow phenomena in clastic intrusions: American Association of Petroleum Geologists Bulletin, v. 50, p. 610–611.

Duranti, D., 2007, Large-scale sand injection in the Paleogene of the North Sea: Modeling of energy and flow velocities, *in* Hurst, A., and Cartwright, J., eds., Sand Injectites: Implications for Hydrocarbon Exploration and Production: American Association of Petroleum Geologists Memoir 87, p. 129–139.

Duranti, D., and Hurst, A., 2004, Fluidization and injection in the deep-water sandstones of the Eocene Alba Formation (UK North Sea): Sedimentology, v. 51, p. 503–529, doi:10.1111/j.1365-3091.2004.00634.x.

Faisst, H., and Eckhardt, B., 2004, Sensitive dependence on initial conditions in transition to turbulence in pipe

flow: Journal of Fluid Mechanics, v. 504, p. 343–352, doi:10.1017/S0022112004008134.

Faules, G., and Boyes, W.H., 2009, Measurement of flow, *in* Boyes, W.H., ed., Instrumentation Reference Book: Burlington, Massachusetts, Butterworth-Heinemann, p. 31–68.

Fineberg, J., and Marder, M., 1999, Instability in dynamic fracture: Physics Reports, v. 313, p. 1–108, doi:10.1016/S0370-1573(98)00085-4.

Flint, S.S., Hodgson, D.M., Sprague, A.R., Brunt, R.L., Van der Merwe, W.C., Figueiredo, J., Prélat, A., Box, D., Di Celma, C., and Kavanagh, J.P., 2011, Depositional architecture and sequence stratigraphy of the Karoo basin floor to shelf edge succession, Laingsburg depocentre, South Africa: Marine and Petroleum Geology, v. 28, p. 658–674, doi:10.1016/j.marpetgeo.2010.06.008.

Fossen, H., 2010, Structural Geology: Cambridge, UK, Cambridge University Press, 463 p.

Hamberg, L., Jepsen, A.M., Borch, N.T., Dam, G., Engkilde, M.K., and Svendsen, J.B., 2007, Mounded structures of injected sandstones in deep-marine Paleocene reservoirs, Cecile Field, Denmark, *in* Hurst, A., and Cartwright, J., eds., Sand Injectites: Implications for Hydrocarbon Exploration and Production: American Association of Petroleum Geologists Memoir 87, p. 69–79.

Hillier, R.D., and Cosgrove, J.W., 2002, Core and seismic observations of overpressure-related deformation within Eocene sediments of the Outer Moray Firth, UKCS: Petroleum Geoscience, v. 8, p. 141–149, doi:10.1144/petgeo.8.2.141.

Hodgson, R.A., 1961, Classification of structures on joint surfaces: American Journal of Science, v. 259, p. 493–502, doi:10.2475/ajs.259.7.493.

Hogg, A.J., 1994, The inertial migration of non-neutrally buoyant spherical particles in two-dimensional shear flows: Journal of Fluid Mechanics, v. 272, p. 285–318, doi:10.1017/S0022112094004477.

Horsrud, P., 2001, Estimating mechanical properties of shale from empirical correlations: Society of Petroleum Engineers Drilling and Completion, v. 16, p. 68–73, doi:10.2118/56017-PA.

Hubbard, S.M., Romans, B.W., and Graham, S.A., 2007, An outcrop example of large-scale conglomeratic intrusions sourced from deep-water channel deposits, Cerro Toro Formation, Magallanes basin, southern Chile, *in* Hurst, A., and Cartwright, J., eds., Sand Injectites: Implications for Hydrocarbon Exploration and Production: American Association of Petroleum Geologists Memoir 87, p. 199–207.

Hull, D., 1996, Interpretation of river line patterns on indentation generated fracture surfaces with comments on fractal characteristics described by Djordjevic et al: Journal of Materials Science Letters, v. 15, p. 651–653, doi:10.1007/BF00264102.

Hurst, A., Cartwright, J., and Duranti, D., 2003, Fluidization structures produced by upward injection of sand through a sealing lithology, *in* Van Rensbergen, P., Hillis, R.R., Maltman, A.J., and Morley, C.K., eds., Subsurface Sediment Mobilization: Geological Society of London Special Publication 216, p. 123–138.

Hurst, A., Cartwright, J.A., Duranti, D., Huuse, M., and Nelson, M., 2005, Sand injectites: An emerging global play in deep-water clastic environments, *in* Doré, A.G., and Vining, B.A., eds., Petroleum Geology: North-West Europe and Global Perspectives—Proceedings of the 6th Petroleum Geology Conference: Geological Society of London Petroleum Geology Conference Series 6, p. 133–144, doi:10.1144/0060133.

Hurst, A., Scott, A., and Vigorito, M., 2011, Physical characteristics of sand injectites: Earth-Science Reviews, v. 106, p. 215–246, doi:10.1016/j.earscirev.2011.02.004.

Huuse, M., Duranti, D., Steinsland, N., Guargena, C.G., Prat, P., Holm, K., Cartwright, J.A., and Hurst, A., 2004, Seismic characteristics of large-scale sandstone intrusions in the Paleogene of the South Viking Graben, UK and Norwegian North Sea, *in* Davies, R.J., Cartwright, J., Stewart, S.A., Underhill, J.R., and Lappin, M., eds., 3D Seismic Technology: Application to the Exploration of Sedimentary Basins: Geological Society of London Memoir 29, p. 263–278.

Huuse, M., Shoulders, S., Netoff, D., and Cartwright, J., 2005, Giant sandstone pipes record basin-scale liquefaction of buried dune sands in the Middle Jurassic of SE Utah: Terra Nova, v. 17, p. 80–85, doi:10.1111/j.1365-3121.2004.00587.x.

Jackson, C., Huuse, M., and Barber, G., 2011, Geometry of winglike clastic intrusions adjacent to a deep-water channel complex: Implications for hydrocarbon exploration and production: American Association of Petroleum Geologists Bulletin, v. 95, p. 559–584, doi:10.1306/09131009157.

Jolly, R.J.H., and Lonergan, L., 2002, Mechanisms and controls on the formation of sand intrusions: Journal of the Geological Society, v. 159, p. 605–617, doi:10.1144/0016-764902-025.

Jones, G.E.D., Hodgson, D.M., and Flint, S.S., 2013, Contrast in the process response of stacked clinothems to the shelf-slope rollover: Geosphere, v. 9, p. 299–316, doi:10.1130/GES00796.1.

Jonk, R., 2010, Sand-rich injectites in the context of short-lived and long-lived fluid flow: Basin Research, v. 22, p. 603–621, doi:10.1111/j.1365-2117.2010.00471.x.

Kane, I.A., 2010, Development and flow structures of sand injectites: The Hind Sandstone Member injectite complex, Carboniferous, UK: Marine and Petroleum Geology, v. 27, p. 1200–1215, doi:10.1016/j.marpetgeo.2010.02.009.

Kawakami, G., and Kawamura, M., 2002, Sediment flow and deformation (SFD) layers: Evidence for intrastratal flow in laminated muddy sediments of the Triassic Osawa Formation, northeast Japan: Journal of Sedimentary Research, v. 79, p. 171–181.

Keighley, D.G., and Pickerill, R.K., 1994, Flute-like marks and associated structures from the Carboniferous Port Hood Formation of eastern Canada: Evidence of secondary origin in association with sediment intrusion: Journal of Sedimentary Research, v. 64, p. 253–263.

Krieger, I.M., and Dougherty, T.J., 1959, A mechanism for non-Newtonian flow in suspension of rigid spheres: Transactions of the Society of Rheology, v. 3, p. 137–152, doi:10.1122/1.548848.

Leva, M., 1959, Fluidization: New York, McGraw-Hill, 327 p.

Lorenz, J.C., Tuefel, L.W., and Warpinski, N.R., 1991, Regional Fractures I: A mechanism for the formation of regional fractures at depth in flat-lying reservoirs: American Association of Petroleum Geologists Bulletin, v. 75, p. 1714–1737.

Lothe, A.E., Borge, H., and Gabrielsen, R.H., 2004, Modelling of hydraulic leakage by pressure and stress simulations and implications for Biot's constant: An example from the Halten Terrace, offshore Mid-Norway: Petroleum Geoscience, v. 10, p. 199–213, doi:10.1144/1354-079303-579.

Lowe, D., 1975, Water escape structures in coarse-grained sediments: Sedimentology, v. 22, p. 157–204, doi:10.1111/j.1365-3091.1975.tb00290.x.

Lutton, R.J., 1970, Tensile fracture mechanics from fracture surface morphology, *in* Clark, G.B., ed., Dynamic Rock Mechanics: 12th U.S. Symposium on Rock Mechanics: Rolla, Missouri, 16–18 November, p. 561–571.

Macdonald, D., and Flecker, R., 2007, Injected sand sills in a strike-slip fault zone: A case study from the Pil'sk Suite (Miocene), southeast Schmidt Peninsula, Sakhalin, *in* Hurst, A., and Cartwright, J., eds., Sand Injectites: Implications for Hydrocarbon Exploration and Production: American Association of Petroleum Geologists Memoir 87, p. 253–263.

Martill, D.M., and Hudson, J.D., 1989, Injection clastic dykes in the Lower Oxford Clay (Jurassic) of central England: Relationship to compaction and concretion formation: Sedimentology, v. 36, p. 1127–1133, doi:10.1111/j.1365-3091.1989.tb01546.x.

Matthews, M.D., 2007, The effect of grain shape and density on size measurement, *in* Syvitski, J.P.M., ed., Principles, Methods and Application of Particle Size Analysis: New York, Cambridge University Press, p. 22–33.

Müller, G., and Dahm, T., 2000, Fracture morphology of tensile cracks and rupture velocity: Journal of Geophysical Research, v. 105, p. 723–738, doi:10.1029/1999JB900314.

Munson, B.R., Rothmayer, A.P., Okiishi, T.H., and Huebsch, W.W., 2012, Fundamentals of Fluid Mechanics (7th edition): Hoboken, New Jersey, John Wiley and Sons, 796 p.

Newsom, J.F., 1903, Clastic dikes: Geological Society of America Bulletin, v. 14, p. 227–268, doi:10.1130/GSAB-14-227.

Nichols, R.J., Sparks, R.S.J., and Wilson, C.J.N., 1994, Experimental studies of the fluidization of layered sediments and the formation of fluid escape structures: Sedimentology, v. 41, p. 233–253, doi:10.1111/j.1365-3091.1994.tb01402.x.

Obermeier, S.F., 1998, Liquefaction evidence for strong earthquakes of Holocene and latest Pleistocene ages in the states of Indiana and Illinois, USA: Engineering Geology, v. 50, p. 227–254, doi:10.1016/S0013-7952(98)00032-5.

Obermeier, S.F., Olson, S.M., and Green, R.A., 2005, Field occurrences of liquefaction-induced features: A primer for engineering geologic analysis of paleoseismic shaking: Engineering Geology, v. 76, p. 209–234, doi:10.1016/j.enggeo.2004.07.009.

Parize, O., and Friès, G., 2003, The Vocontian clastic dykes and sills: A geometric model, *in* Van Rensbergen, P., Hillis, R.R., Maltman, A.J., and Morley, C.K., eds., Subsurface Sediment Mobilization: Geological Society of London Special Publication 216, p. 51–72.

Parize, O., Beaudoin, B., Champanhet, J.-M., Friès, G., Imbert, P., Labourdette, R., Paternoster, B., Rubino, J.-L., and Schneider, F., 2007, A methodological approach to clastic injectites: From field analysis to seismic modelling—Examples of Vocontian Aptian and Albian injectites (Southwest France), *in* Hurst, A., and Cartwright, J., eds., Sand Injectites: Implications for Hydrocarbon Exploration and Production: American Association of Petroleum Geologists Memoir 87, p. 173–183.

Peterson, G.L., 1968, Flow structures in sandstone dikes: Sedimentary Geology, v. 2, p. 177–190, doi:10.1016/0037-0738(68)90024-9.

Phillips, W.J., 1972, Hydraulic fracturing and mineralization: Journal of the Geological Society, v. 128, p. 337–359, doi:10.1144/gsjgs.128.4.0337.

Pollard, W.J., Muller, O.H., and Dockstader, D.R., 1975, The form and growth of fingered sheet intrusions: Geological Society of America Bulletin, v. 86, p. 351–363, doi:10.1130/0016-7606(1975)86<351:TFAGOF>2.0.CO;2.

Pollard, D.D., Segall, P., and Delaney, P.T., 1982, Formation and interpretation of dilatant echelon cracks: Geological Society of America Bulletin, v. 93, p. 1291–1301, doi:10.1130/0016-7606(1982)93<1291:FAIODE>2.0.CO;2.

Post, S., 2011, Applied and Computational Fluid Mechanics: Sudbury, Massachusetts, Jones and Bartlett Publishers, 600 p.

Prélat, A., and Hodgson, D.M., 2013, The full range of turbidite bed thickness patterns in submarine lobes: Controls and implications: Journal of the Geological Society, v. 170, p. 209–214, doi:10.1144/jsgs2012-056.

Quigley, M.C., Bastin, S., and Bradley, B.A., 2013, Recurrent liquefaction in Christchurch, New Zealand, during the Canterbury earthquake sequence: Geology, v. 41, p. 419–422, doi:10.1130/G33944.1.

Rieke, H.H., III, and Chilingarian, G.V., 1974, Compaction of Argillaceous Sediments: Amsterdam, Elsevier, Developments in Sedimentology, v. 16, 424 p.

Ross, J.A., Peakall, J., and Keevil, G.M., 2011, An integrated model of extrusive sand injectites in cohesionless sediments: Sedimentology, v. 58, p. 1693–1715, doi:10.1111/j.1365-3091.2011.01230.x.

Ross, J.A., Peakall, J., and Keevil, G.M., 2013, Sub-aqueous sand extrusion dynamics: Journal of the Geological Society, v. 170, p. 593–602, doi:10.1144/jgs2012-124.

Ross, J.A., Peakall, J., and Keevil, G.M., 2014, Facies and flow regimes of sandstone-hosted columnar intrusions: Insights from the pipes of Kodachrome Basin State Park: Sedimentology, v. 61, p. 1764–1792, doi:10.1111/sed.12115.

Rubin, A.M., 1995, Propagation of magma-filled cracks: Annual Review of Earth and Planetary Sciences, v. 23, p. 287–336, doi:10.1146/annurev.ea.23.050195.001443.

Schofield, N.J., Brown, D.J., Magee, C., and Stevenson, C.T., 2012, Sill morphology and comparison of brittle and non-brittle emplacement mechanism: Journal of

the Geological Society, v. 169, p. 127–141, doi:10 .1144/0016-76492011-078.

Schwab, A.M., Jameson, E.W., and Townsley, A., 2014, Volund Field: Development of an Eocene sandstone injection complex, offshore Norway, *in* McKie, T., Rose, P.T.S., Hartley, A.J., Jones, D.W., and Armstrong, T.L., eds., Tertiary Deep-Marine Reservoirs of the North Sea Region: Geological Society of London Special Publication 403, doi:10.1144/SP403.4 (in press).

Scott, A., Vigorito, M., and Hurst, A., 2009, The process of sand injection: Internal structures and relationships with host strata (Yellowbank Creek Injectite Complex, California, U.S.A.): Journal of Sedimentary Research, v. 79, p. 568–583, doi:10.2110/jsr.2009.062.

Scott, A., Hurst, A., and Vigorito, M., 2013, Outcrop-based reservoir characterization of a kilometer-scale sand-injectite complex: American Association of Petroleum Geologists Bulletin, v. 97, p. 309–343, doi:10.1306/05141211184.

Secor, D.T., 1965, Role of fluid pressure in jointing: American Journal of Science, v. 263, p. 633–646, doi:10 .2475/ajs.263.8.633.

Segré, G., and Silberberg, A., 1962a, Behaviour of macroscopic rigid spheres in Poiseuille flow. Part 1. Determination of local concentration by statistical analysis of particle passages through crossed light beams: Journal of Fluid Mechanics, v. 14, p. 115–135, doi:10.1017 /S002211206200110X.

Segré, G., and Silberberg, A., 1962b, Behaviour of macroscopic rigid spheres in Poiseuille flow. Part 2. Experimental results and interpretation: Journal of Fluid Mechanics, v. 14, p. 136–157, doi:10.1017 /S0022112062001111.

Sharon, E., Gross, S.T., and Fineberg, J., 1995, Local crack branching as a mechanism for instability in dynamic fracture: Physical Review Letters, v. 74, p. 5096–5099, doi:10.1103/PhysRevLett.74.5096.

Sherry, T.J., Rowe, C.D., Kirkpatrick, J.D., and Brodsky, E.E., 2012, Emplacement and dewatering of the world's largest exposed sand injectite complex: Geochemistry Geophysics Geosystems, v. 13, p. 1–17, doi: 10.1029/2012GC004157.

Singhal, B.B.S., and Gupta, R.P., 1999, Applied Hydrogeology of Fractured Rocks: Dordrecht, The Netherlands, Kluwer Academic Publishers, 400 p.

Sixsmith, P.J., Flint, S.S., Wickens, H.DeV., and Johnson, S.D., 2004, Anatomy and stratigraphic development of a basin floor turbidite system in the Laingsburg Formation, main Karoo Basin, South Africa: Journal of Sedimentary Research, v. 74, p. 239–254, doi:10.1306 /082903740239.

Sommer, E., 1969, Formation of fracture 'lances' in glass: Engineering Fracture Mechanics, v. 1, p. 539–546, doi: 10.1016/0013-7944(69)90010-1.

Sturkell, E.F.F., and Ormö, J., 1997, Impact-related injections in the marine Ordovician Lockne impact structure, Central Sweden: Sedimentology, v. 44, p. 793–804, doi:10 .1046/j.1365-3091.1997.d01-54.x.

Surlyk, F., and Noe-Nygaard, N., 2001, Sand remobilisation and intrusion in the Upper Jurassic Hareelv Formation of East Greenland: Bulletin of the Geological Society of Denmark, v. 48, p. 169–188.

Surlyk, F., Gjelberg, J., and Noe-Nygaard, N., 2007, The Upper Jurassic Hareelv Formation of east Greenland: A giant sedimentary injection complex, *in* Hurst, A., and Cartwright, J., eds., Sand Injectites: Implications for Hydrocarbon Exploration and Production: American Association of Petroleum Geologists Memoir 87, p. 141–149.

Szarawarska, E., Huuse, M., Hurst, A., De Boer, W., Lu, L., Molyneux, S., and Rawlinson, P., 2010, Three-dimensional seismic characterisation of large-scale sandstone intrusions in the lower Palaeogene of the North Sea: Completely injected vs. in situ remobilised sandbodies: Basin Research, v. 22, p. 517–532, doi:10.1111/j.1365 -2117.2010.00469.x.

Taylor, B.J., 1982, Sedimentary dykes, pipes and related structures in the Mesozoic sediments of south-eastern Alexander Island: British Antarctic Survey Bulletin, v. 51, p. 1–42.

Thompson, B., Garrison, R., and Moore, J., 2007, A reservoir-scale Miocene injectite near Santa Cruz, California, *in* Hurst, A., and Cartwright, J., eds., Sand Injectites:

Implications for Hydrocarbon Exploration and Production: American Association of Petroleum Geologists Memoir 87, p. 151–162.

Truswell, J.F., 1972, Sandstone sheets and related intrusions from Coffee Bay, Transkei, South Africa: Journal of Sedimentary Petrology, v. 42, p. 578–583, doi:10.1306 /74D725C2-2B21-11D7-8648000102C1865D.

van der Merwe, W.C., Flint, S.S., and Hodgson, D.M., 2010, Sequence stratigraphy of an argillaceous, deepwater basin-plain succession: Vischkuil Formation (Permian), Karoo Basin, South Africa: Marine and Petroleum Geology, v. 27, p. 321–333, doi:10.1016/j .marpetgeo.2009.10.007.

Vétel, W., and Cartwright, J., 2010, Emplacement mechanics of sandstone intrusions: Insights from the Panoche Giant Injection Complex, California: Basin Research, v. 22, p. 783–807, doi:10.1111/j.1365-2117.2009 .00439.x.

Vigorito, M., and Hurst, A., 2010, Regional sand injectite architecture as a record of pore-pressure evolution and sand redistribution in the shallow crust: Insights from the Panoche Giant Injection Complex, California: Journal of the Geological Society, v. 167, p. 889–904, doi:10.1144/0016-76492010-004.

Vigorito, M., Hurst, A., Cartwright, J., and Scott, A., 2008, Regional-scale subsurface sand remobilization: Geometry and architecture: Journal of the Geological Society, v. 165, p. 609–612, doi:10.1144/0016-76492007 -096.

Woodworth, J.B., 1895, Some features on joints: Science, v. 2, p. 903–904.